Multiple-electron ionization, capture, and loss by 19-MeV F^{q+} (q=2–9) in collisions with Ne and Ar

O. Heber,* G. Sampoll,† B. B. Bandong,‡ R. J. Maurer,† and R. L. Watson
Cyclotron Institute and Department of Chemistry, Texas A&M University, College Station, Texas 77843

I. Ben-Itzhak, J. M. Sanders,§ J. L. Shinpaugh,‖ and P. Richard
J. R. MacDonald Laboratory, Kansas State University, Manhattan, Kansas 66506
(Received 23 March 1995)

Charge-exchange processes in fast collisions of F^{q+} (q=2–9) on Ne and Ar gas targets have been studied using the projectile–recoil-ion coincidence method. The target ionization without a projectile charge change increases with increasing projectile charge approximately as $\sim q^{1.4}$. This dependence is weaker than the q^2 dependence predicted by the first Born approximation because of the large ionization probabilities involved. The single-electron-capture cross sections follow the known q^3 scaling law, while the double-electron-capture cross sections display a q^6 dependence, as predicted by the independent-electron approximation for small capture probabilities. Single- and double-electron loss from the L shell decreases with increasing q mainly because of the decrease in the number of L-shell electrons, while binding-energy effects play only a minor role. In contrast, the large sudden decrease in electron-loss cross sections once K-shell electrons must be removed is due to the large increase in binding energy.

PACS number(s): 34.50.Fa, 34.70.+e

I. INTRODUCTION

Atomic collisions between fast highly charged projectile ions and atomic gas targets provide an efficient method for producing cold highly charged recoil ions [1]. The recoil-ion charge distribution has been found to be highly dependent on the postcollision charge of the projectile [2–6]. This dependence has been attributed in fast collisions to an impact-parameter selection effect [2]. For example, ionization is associated mostly with soft collisions at large impact parameters, whereas electron capture occurs at smaller impact parameters. For projectiles with charges higher than $q=10$, the cross section for recoil-ion production increases rapidly with the projectile charge, whereas the recoil-ion-charge distribution stays approximately constant [7].

Cross sections for charge-exchange processes are needed for various applications, such as the investigation of plasma dynamics, the Tokamak and accelerator design, and the study of interstellar media. The lack of available theoretical or experimental cross sections for a particular collision system is commonly circumvented through the use of scaling laws. These laws approximate the dependence of cross sections for a certain process on the collision parameters. A commonly used scaling law for single-electron capture was derived by Knudsen, Haugen, and Hvelplund [8] and is based on the classical theory of Bohr and Lindhard [9]. Using an empirical approach, Schlachter *et al.* [10] found a somewhat different scaling law for the same process. A theoretical study by Crothers and Todd [11] predicted a q^3 scaling for one-electron capture at medium velocities [12]. Be *et al.* [13] derived an empirical power scaling law for net ionization, and a one-electron-loss scaling law has been the subject of

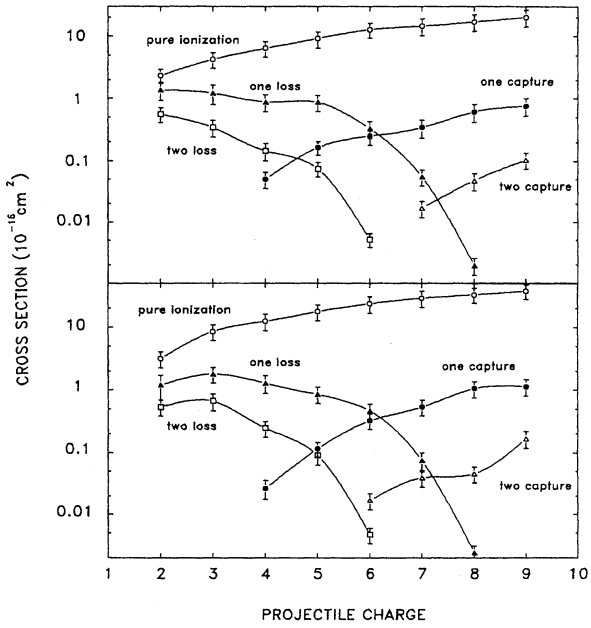

FIG. 1. Cross sections for pure target ionization, electron capture, and electron loss in collisions of F^{q+} (q=2–9) with Ar (bottom) and Ne (top) as a function of the projectile charge. The lines are to guide the eye.

*Present address: Department of Particle Physics, Weizmann Institute of Science, Rehovot, Israel.
†Present address: EG&G Energy Measurements, P.O. Box 380, Suitland, MD 20752.
‡Present address: Nuclear Chemistry Division, Lawrence Livermore National Laboratory, L396, Livermore, CA 94550.
§Present address: University of South Alabama, Mobile, AL 36688.
‖Present address: East Carolina University, Greenville, NC 27858.

TABLE I. Total cross sections for electron loss, capture, and pure target ionization in F^{q+} + Ne collision at 19 MeV (in units of 10^{-16} cm^2).

Projectile charge	Pure ionization	One-capture	Two-capture	One-loss	Two-loss
2	2.364			1.369 5	0.555 1
3	4.261			1.218 8	0.341 0
4	6.447	0.05		0.880 4	0.143 6
5	9.212	0.162 8		0.876 1	0.074 1
6	12.858	0.251 3		0.329 9	0.005 1
7	14.638	0.342 9	0.016 8	0.054 9	
8	17.113	0.612 2	0.047 5	0.001 9	
9	20.283	0.762 8	0.103 1		

TABLE II. Total cross sections for electron loss, capture, and pure target ionization in F^{q+} + Ar collision at 19 MeV (in units of 10^{-16} cm^2).

Projectile charge	Pure ionization	One-capture	Two-capture	One-loss	Two-loss
2	3.150			1.189	0.532 9
3	8.437			1.783	0.667 8
4	12.289	0.026 5		1.282	0.245 9
5	17.564	0.115		0.854 3	0.090 5
6	23.565	0.322	0.016 8	0.465 7	0.004 7
7	28.838	0.537	0.039 7	0.074 7	
8	32.993	1.05	0.045 9	0.002 4	
9	37.994	1.13	0.167 5		

TABLE III. Relative recoil-ion yield distribution for pure Ar target ionization.

	Projectile charge							
Ar charge	2	3	4	5	6	7	8	9
1	0.855(3)	0.863(2)	0.832(2)	0.784(2)	0.765(2)	0.735(1)	0.725(2)	0.713(2)
2	0.095(1)	0.108 0(6)	0.125 0(9)	0.147 1(9)	0.160 5(7)	0.171 0(7)	0.177(1)	0.182(1)
3	0.013 6(4)	0.017 6(2)	0.025 2(4)	0.036 3(5)	0.044 8(4)	0.055 8(4)	0.063 2(6)	0.067 2(8)
4	0.003 3(2)	0.004 1(1)	0.006 5(2)	0.010 3(3)	0.012 7(2)	0.016 2(2)	0.020 8(3)	0.023 7(5)
5	0.001 5(1)	0.002 80(9)	0.004 8(2)	0.007 1(2)	0.007 0(2)	0.006 9(2)	0.007 1(2)	0.007 6(3)
6	0.001 0(1)	0.002 30(8)	0.002 5(2)	0.005 3(2)	0. 004 8(1)	0.005 9(2)	0.003 7(2)	0.003 4(2)
7	0.000 40(7)	0.001 06(6)	0.002 2(1)	0.003 1(2)	0.002 5(1)	0.003 9(1)	0.001 9(1)	0.001 7(2)
8	0.000 24(5)	0.000 46(4)	0.001 27(9)	0.001 9(1)	0.002 21(8)	0.002 80(9)	0.000 81(7)	0.000 65(7)
9	0.000 21(5)	0.000 27(3)	0.000 57(6)	0.000 95(8)	0.000 65(5)	0.001 42(7)	0.000 21(4)	0.000 15(3)
10			0.000 23(4)	0.000 52(6)	0.000 13(2)	0.000 75(5)	0.000 15(3)	0.000 06(2)

TABLE IV. Relative Ar recoil-ion-yield distribution for one-electron capture by the projectile F^{q+}.

	Projectile charge					
Ar charge	4	5	6	7	8	9
1		0.003(4)				
2	0.086(3)	0.048(3)	0.024(2)	0.008(1)	0.024(1)	
3	0.190(2)	0.121(4)	0.081(2)	0.060(1)	0.035 1(6)	0.026(2)
4	0.247(4)	0.199(5)	0.164(2)	0.135(2)	0.096 2(8)	0.086(2)
5	0.209(4)	0.215(5)	0.227(3)	0.227(2)	0.189(1)	0.178(2)
6	0.121(3)	0.153(4)	0.193(2)	0.208(2)	0.221(1)	0.241(3)
7	0.080(3)	0.130(4)	0.157(2)	0.179(2)	0.202(1)	0.220(3)
8	0.050(2)	0.098(3)	0.107(2)	0.139(2)	0.157(2)	0.169(2)
9	0.013(1)	0.022(2)	0.044(1)	0.0404(8)	0.065 3(6)	0.065(2)
10	0.002 9(5)	0.010(1)	0.003 1(3)	0.003 3(2)	0.010 4(3)	0.014 7(6)
11	0.001 5(3)			0.001 1(2)	0.001 18(8)	0.001 1(2)

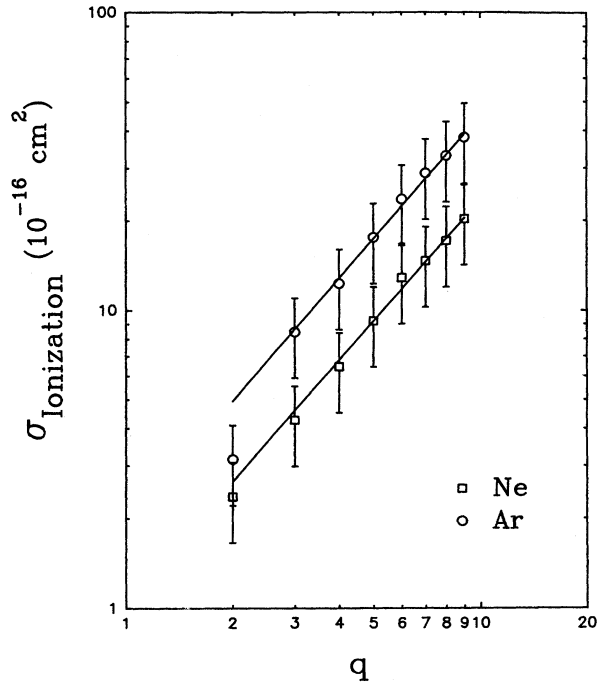

FIG. 2. Pure ionization cross section as a function of the projectile charge. The lines are the best fits using the scaling law referred to in the text.

studies by Graham *et al.* [14].

It is useful to have scaling laws for all charge-exchange processes, including multiple-electron processes, such as double-electron capture and loss, to provide simple and accurate estimates of cross sections over a wide range of energies, projectile charges, and target atomic numbers. Another useful approach for evaluating cross sections of multielectronic processes is the independent-electron approximation. In this method, the probability of a given process as a function of the impact parameter $p(b)$ is calculated for one active electron while all others are treated as spectators. The probability $P_n(b)$ of the same process occurring to n electrons out of the N equivalent electrons of the system is given by the binomial distribution [15] $p_n(b)=\binom{N}{n}p^n(b)\times[1-p(b)]^{N-n}$. Using this probability function, the cross section can be evaluated by integrating over the whole impact-parameter range

$$\sigma_n=2\pi\int_0^\infty b\,db\,P_n(b). \tag{1}$$

Expressions for ionization, electron capture, and electron loss were presented in detail in an earlier work [16], and by employing the independent-electron approximation, predictions were made concerning the dependence of multielectron processes on the projectile charge.

The aim of the present work was to investigate cross sections for charge exchange as a function of the incident projectile charge. The collision systems studied were F^{q+} + Ne and Ar for $q=2-9$ at 1 MeV/amu. The experimental method is briefly described in Sec. II, and the dependences of the difference processes (i.e., ionization, electron capture, and electron loss) on the projectile charge are discussed in Sec. III.

TABLE V. Relative Ar recoil-ion-yield charge-state distribution for two-electron capture by the projectile F^{q+}.

	Projectile charge			
Ar charge	6	7	8	9
2	0.006(5)			
3	0.004(3)	0.004(2)	0.005(2)	0.007(3)
4	0.029(4)	0.016(1)	0.008(1)	0.013(2)
5	0.085(6)	0.047(2)	0.026(2)	0.021(2)
6	0.165(8)	0.135(4)	0.064(3)	0.072(3)
7	0.26(1)	0.270(5)	0.185(4)	0.179(5)
8	0.29(1)	0.307(6)	0.325(5)	0.309(6)
9	0.131(7)	0.197(5)	0.256(5)	0.307(6)
10	0.025(3)	0.024(2)	0.102(3)	0.103(4)
11	0.003(1)		0.028(2)	

II. EXPERIMENT

A well-defined beam of 1-MeV/amu F^{q+} ($q=2-9$) from the Kansas State University, J. R. MacDonald Laboratory EN Tandem accelerator, was directed into a doubly differentially

TABLE VI. Relative Ar recoil-ion-yield distribution for one-electron loss by the projectile F^{q+}.

	Projectile charge						
Ar charge	2	3	4	5	6	7	8
1	0.472(3)	0.339(3)	0.227(2)	0.155(2)	0.098(2)	0.009(4)	
2	0.325(2)	0.332(2)	0.302(2)	0.252(2)	0.187(1)	0.127(3)	0.05(3)
3	0.109(2)	0.156(2)	0.198(2)	0.239(2)	0.255(2)	0.229(3)	0.00(2)
4	0.050 6(8)	0.071(1)	0.096 4(8)	0.132(2)	0.163 2(9)	0.201(3)	0.09(2)
5	0.021 9(5)	0.043 7(8)	0.067 7(7)	0.088(1)	0.107 7(7)	0.133(2)	0.13(2)
6	0.010 9(4)	0.026 8(6)	0.046 5(6)	0.063 5(9)	0.077 9(6)	0.093(2)	0.24(3)
7	0.006 2(3)	0.017 3(5)	0.033 (5)	0.040 4(8)	0.057 3(6)	0.070(2)	0.20(3)
8	0.003 6(2)	0.010 8(4)	0.021 9(4)	0.024 5(6)	0.040 9(5)	0.048(2)	0.20(3)
9	0.000 47(8)	0.002 1(2)	0.004 7(2)	0.004 9(3)	0.010 7(3)	0.007 6(5)	0.090(2)
10	0.000 32(7)	0.000 29(7)	0.000 85(8)	0.000 8(2)	0.001 13(8)	0.000 8(2)	
11			0.000 39(5)	0.000 27(15)			

TABLE VII. Relative Ar recoil-ion-yield distribution for two-electron loss by the projectile F^{q+}.

	Projectile charge				
Ar charge	2	3	4	5	6
1	0.206(3)	0.136(3)	0.091(3)	0.029(6)	
2	0.298(3)	0.230(3)	0.160(3)	0.112(5)	0.031(9)
3	0.194(3)	0.195(3)	0.184(3)	0.166(5)	0.048(8)
4	0.112(2)	0.133(3)	0.140(3)	0.141(4)	0.073(9)
5	0.082(2)	0.107(2)	0.137(3)	0.145(5)	0.18(1)
6	0.052(2)	0.081(2)	0.123(2)	0.139(4)	0.19(1)
7	0.035(1)	0.064(2)	0.099(2)	0.138(4)	0.24(1)
8	0.016 4(7)	0.042(2)	0.054(2)	0.093(3)	0.17(1)
9	0.003 1(3)	0.009 5(6)	0.008 7(6)	0.031(2)	0.064(6)
10	0.000 7(2)	0.001 6(3)	0.000 8(2)	0.005 3(9)	0.008(2)
11		0.000 8(2)			

pumped gas target cell. The incoming projectile charge was selected by an analyzing magnet and an additional cleanup magnet before the target cell was used to minimize impurity charge states produced by collisions with the residual gas. A magnet behind the target cell exit separated the outgoing projectile charge states, which were detected by a position-sensitive parallel-plate avalanche detector (PPAD).

Recoil ions produced in projectile-target atom collisions were extracted by means of a transverse electric field, which accelerated them toward a microchannel plate detector in a time-of-flight recoil-ion spectrometer. The recoil-ion signal was used to start a time-to-amplitude converter, while a fast timing signal from the projectile detector (PPAD) was used to stop it. A more detailed description of this experimental setup has been published elsewhere [17].

To measure electron-capture and electron-loss cross sections, which are orders of magnitude smaller than the pure ionization cross section, the direct beam was blocked by a shutter in front of the projectile detector to allow the beam current to be increased. Pressure-dependence measurements were performed to verify that single-collision conditions existed for both projectiles and recoil ions. The working pressure in the target cell was 0.8 mTorr, whereas the background pressure in the beam line was less than 10^{-7} Torr.

Total cross sections were calculated by normalizing the recoil-ion yields to previously measured pure ionization cross sections for O^{8+} ions on Ar [18]. The errors associated with the total cross sections are estimated to be 30%. The errors in the relative yields are mainly due to corrections for multiple collisions, and they are of the order of 10% for pure ionization and about 30% for the low charge states produced by electron capture and the high charge states produced by electron loss. The errors in relative yields are given in the tables presented in Sec. III.

III. RESULTS AND DISCUSSION

The collision processes under investigation were

$$F^{q+} + Ar \rightarrow F^{q'} + Ar^{m+} + (q' + m - q)e^-$$

and the corresponding processes for a Ne target. Of special interest are the total cross sections for pure target ionization

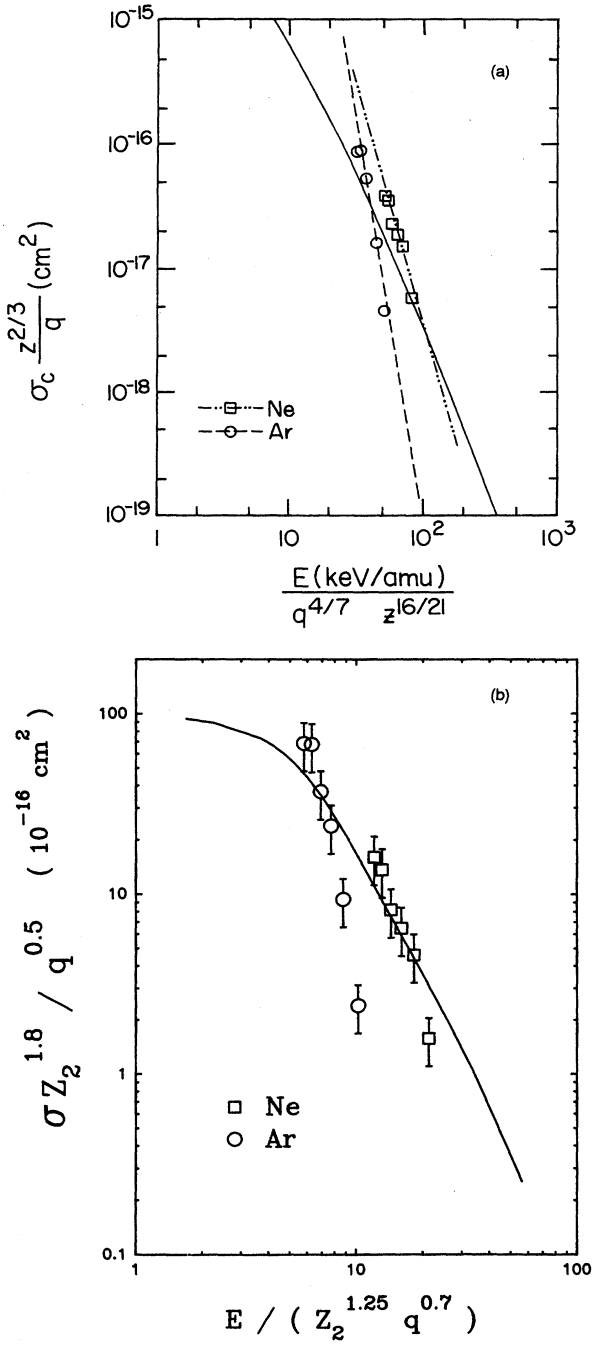

FIG. 3. Single-electron-capture cross sections compared to (a) Knudsen scaling law and (b) Schlachter scaling law, where q is the projectile charge state and z is the target atomic number.

($q=q'$), for target ionization plus single- and double-electron capture ($q'=q+1,q+2$), and for target ionization plus single- and double-electron loss ($q'=q-1,q-2$), which are shown in Fig. 1. It is apparent that pure target ionization is the most probable process. Electron loss decreases with increasing q, whereas electron capture increases with increasing q. The total cross sections for these channels are presented in Tables I and II.

The general trend for the Ne and Ar cross sections is

TABLE VIII. Relative recoil-ion-yield distribution for pure Ne target ionization.

Ne charge	Projectile charge							
	2	3	4	5	6	7	8	9
1	0.854(6)	0.829(4)	0.796(3)	0.768(3)	0.747(3)	0.725(3)	0.718(3)	0.709(3)
2	0.112(3)	0.129(2)	0.145(1)	0.145(1)	0.165(1)	0.173(2)	0.175(1)	0.178(2)
3	0.025 1(1)	0.032 2(8)	0.042 3(6)	0.052 2(7)	0.059 1(7)	0.067 4(8)	0.068 2(8)	0.070 5(9)
4	0.005 8(5)	0.008 1(4)	0.013 0(3)	0.018 4(4)	0.022 2(5)	0.026 4(5)	0.027 9(5)	0.029 7(6)
5	0.001 4(2)	0.001 3(2)	0.003 2(2)	0.004 2(2)	0.005 4(2)	0.007 5(3)	0.008 6(3)	0.010 1(4)
6	0.000 5(2)	0.000 4(1)	0.000 39(5)	0.000 91(9)	0.001 1(1)	0.000 86(9)	0.001 4(1)	0.001 8(2)
7			0.000 18(4)	0.000 14(4)	0.000 16(4)	0.000 20(4)	0.000 10(3)	0.000 15(4)

similar for all the processes. The most significant difference between the Ne and Ar targets is in the pure target ionization channel. The cross sections for pure target ionization of Ar are about a factor of 2 larger than those of Ne. Most of the ionized electrons are removed from the outer shell, which contains the same number of electrons in both cases [19]. Pure target ionization is more probable for Ar than for Ne because its electrons are moving in a central field having a lower effective Z (as is reflected by the fact that the average eight outer-electron binding energies are 19 eV for Ar and 28 eV for Ne).

The recoil-ion-charge distributions are given in Tables III–XII for each cross section presented in Fig. 1 (and Tables I and II). The errors included in the tables are relative and due mainly to corrections for multiple collision. The partial cross sections for each projectile recoil-ion combination are obtained upon multiplying the cross sections in Tables I and II by the respective probabilities in Tables III–XII.

A. Pure ionization

The pure ionization cross sections as functions of projectile charge are shown in Fig. 2. These cross sections were fitted to a power-law dependence on the projectile charge as suggested by Be *et al.* [13]

$$\sigma_i = \sigma_0 q^{\alpha}. \tag{2}$$

For the Ne target, the best fit of Eq. (2) gives $\alpha = 1.36 \pm 0.06$ and $\sigma_0 = (1.0 \pm 0.1) \times 10^{-16}$ cm^2. A similar fit for the Ar target gives $\alpha = 1.37 \pm 0.06$ and $\sigma_0 = 1.9 \pm 0.2 \times 10^{-16}$ cm^2. These results are in good agreement with the results of Be *et al.* [13], although the values of α differs slightly from their value of $\alpha = 1.48$. It can be seen clearly in Fig. 2 that both sets of data are characterized by the same value of α even though the magnitudes of the cross sections differ from one another by about a factor of 2.

A q^2 scaling law should be expected for $p_i(b)$ from the first Born approximation. Thus the multielectron ionization cross section should scale as

$$\sigma_n = 2\pi \binom{N}{n} \int_0^{\infty} b\, db [q^2 p_i(b)]^n [1 - q^2 p_i(b)]^{N-n}. \tag{3}$$

Once $q^2 p_i(b)$ is comparable to 1, the term $[1 - q^2 p_i(b)]^{N-n}$ will reduce the cross sections for n-electron ionization and will weaken the q^2 dependence, as is the case in the present measurements. On the other hand, for $Nq^2 p_i(b) \ll 1$, the cross sections should scale as q^{2n} [20]. As a result of this effect, the contribution to the total cross section from the range of impact parameters where the perturbative approach fails is negligible and one can use it approximately [20].

B. Electron capture

The single-capture cross sections are compared to predictions of the scaling laws of Knudsen *et al.* [8] and Schlachter *et al.* [10] in Figs. 3(a) and 3(b), respectively. Both scaling laws are in reasonable agreement with the experimental values. The best power-law fit to the data gives a steeper slope than the two scaling laws, especially that of Schlachter *et al.*

Another approach to single-electron capture suggests a q^3 scaling as first predicted by Bohr [21], using a classical model. Crothers and Todd [11] showed that q^3 scaling is pre-

TABLE IX. Relative Ne recoil-ion-yield distribution for one-electron capture by the projectile F^{q+}.

Ne charge	Projectile charge					
	4	5	6	7	8	9
1	0.162(2)	0.116(2)	0.091(1)	0.066(2)	0.056(2)	0.033(2)
2	0.325(2)	0.266(2)	0.210(2)	0.165(2)	0.126(2)	0.112(2)
3	0.289(2)	0.302(2)	0.296(2)	0.271(2)	0.230(2)	0.229(2)
4	0.162(1)	0.214(2)	0.254(2)	0.277(2)	0.272(2)	0.280(2)
5	0.049 9(7)	0.084 4(9)	0.123(3)	0.159(2)	0.195(2)	0.214(2)
6	0.008 9(3)	0.015 4(4)	0.021 6(5)	0.046 0(8)	0.085 8(9)	0.093(1)
7	0.001 5(1)	0.003 0(2)	0.002 9(2)	0.014 5(4)	0.012 4(6)	0.010 5(7)
8	0.001 0(1)		0.000 91(9)	0.000 9(1)	0.002 6(2)	0.007 7(3)

TABLE X. Relative Ne recoil-ion-yield distribution for two-electron capture by the projectile F^{q+}.

	Projectile charge		
Ne charge	7	8	9
2	0.016(3)	0.009(3)	0.006(2)
3	0.090(5)	0.028(2)	0.024(2)
4	0.188(7)	0.073(4)	0.070(3)
5	0.324(9)	0.189(5)	0.162(4)
6	0.231(8)	0.327(7)	0.257(6)
7	0.110(5)	0.323(7)	0.345(6)
8	0.027(3)	0.042(3)	0.136(4)
9	0.004(1)		

dicted by several different quantum-mechanical theoretical approaches, and Tawara [6] has shown that this scaling law is valid for collisions with He targets. The present single-electron-capture cross sections divided by q^3 are plotted as a function of q in Fig. 4.

Double-electron capture is expected to scale as q^6 within the independent-electron approximation as long as $p_c(b) \ll 1$. The double-electron-capture cross sections divided by q^6 are also shown in Fig. 4. The single- and double-electron capture follow these scaling laws reasonably well except at low q values. This is not surprising since these scaling laws were derived for bare projectiles. The effect of electron capture and Auger decay is discussed in a previous publication [19].

C. Electron loss

The cross sections for single- and double-electron loss by 1-MeV/amu fluorine ions colliding with Ne and Ar targets behave similarly as a function of projectile charge. The electron-loss cross sections are slightly larger for the Ar target because of its lower effective charge. These cross sections, shown in Fig. 5, decrease slowly with increasing projectile charge as long as projectile L-shell electrons are available. Electrons in the L shell are more likely to be ionized than K-shell electrons because of their lower binding energy. Once the projectile has only K-shell electrons, the electron-loss cross section decreases rapidly. Such shell effects have been seen before for fast highly charged ions, such as iron ($q=20$–25), by Berkner *et al.* [22], and vanadium ($q=18$–22), by Graham *et al.* [14]. For those fast highly

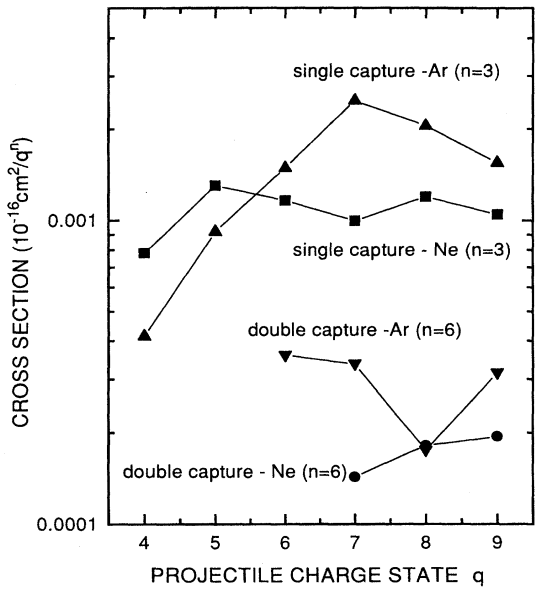

FIG. 4. Single-electron-capture cross section divided by q^3 and double-electron-capture cross section divided by q^6 as a function of the projectile charge. The two-electron-capture data are multiplied by 10^3 to compare all the data on the same scale.

charged ions, the single-electron-loss cross sections decrease approximately according to a $q^{12\pm1}$ scaling law. However, there is pronounced discontinuity between $q=20$ and $q=21$ for vanadium, and between $q=23$ and $q=24$ for iron. This dramatic decrease in the electron-loss cross sections is a definite shell effect caused by the large increase in the ionization potential in going from the L shell to the K shell. The present data for F^{q+} on Ne and Ar show similar shell effects between $q=6$ and $q=7$, but the L-shell electron-loss cross sections decrease slowly compared to the rapid $q^{12\pm1}$ decrease found for highly charged iron and vanadium. This difference may be a consequence of the fact that the ionization potentials for sequential removal of L-shell electrons from fluorine ions increase much more slowly than for the removal of L-shell electrons from highly charged iron and vanadium ions. Electron loss from the valence L shell of the fluorine ions decreases with increasing charge because of the increase in ionization potential and the decreases in the number of available L-shell electrons. The relative importance of

TABLE XI. Relative Ne recoil-ion-yield distribution for one-electron loss by the projectile F^{q+}.

	Projectile charge						
Ne charge	2	3	4	5	6	7	8
1	0.485(3)	0.367(3)	0.265(1)	0.178(2)	0.135(1)	0.084(4)	0.07(3)
2	0.315(2)	0.335(3)	0.324(1)	0.285(1)	0.234(2)	0.155(4)	0.04(2)
3	0.139(2)	0.198(2)	0.252(1)	0.298(2)	0.301(2)	0.283(5)	0.09(2)
4	0.048(9)	0.079(1)	0.123(1)	0.180(1)	0.234(1)	0.295(5)	0.34(5)
5	0.010 9(4)	0.018 3(6)	0.031 4(4)	0.0503(6)	0.0847(8)	0.149(3)	0.38(4)
6	0.001 7(2)	0.002 1(2)	0.004 2(2)	0.007 2(2)	0.009 5(3)	0.029(2)	0.09(2)
7	0.000 41(8)	0.000 2(1)	0.000 65(6)	0.001 6(1)	0.002 4(1)	0.004 8(6)	
8			0.000 30(4)			0.000 5(2)	

TABLE XII. Relative Ne recoil-ion-yield distribution for two-electron loss by the projectile F^{q+}.

	Projectile charge				
Ne charge	2	3	4	5	6
1	0.228(3)	0.165(4)	0.121(2)	0.087(3)	0.059(8)
2	0.326(4)	0.300(5)	0.239(3)	0.158(4)	0.066(7)
3	0.278(3)	0.304(5)	0.329(3)	0.316(5)	0.24(1)
4	0.132(3)	0.177(4)	0.227(3)	0.313(5)	0.36(1)
5	0.030(1)	0.043(2)	0.066(2)	0.105(3)	0.24(1)
6	0.005 2(5)	0.008 8(8)	0.012 7(6)	0.020(1)	0.028(4)
7	0.000 5(2)	0.001 2(3)	0.003 0(3)		0.006(2)
8	0.000 2(1)		0.002 0(3)		

these two effects can be assessed by using the independent-electron approximation. In this approximation, the single-electron-loss cross section can be written as

$$\sigma_{1-\text{loss}} = 2\pi \binom{N}{1} \int_0^\infty b\, db\, p_{\text{loss}}(b)[1-p_{\text{loss}}(b)]^{N-1}$$

$$\cong \frac{N!}{(N-1)!}\sigma_0 = N\sigma_0, \tag{4}$$

where N is the number of L-shell equivalent electrons. Now, assuming that $p_{\text{loss}}(b)$ does not change significantly as a function of the ionization potential, the single-electron-loss cross section should scale with the number of L-shell electrons. A fit using this scaling (i.e., $\sigma_{1-\text{loss}} \cong N\sigma_0$, where σ_0 is an adjustable parameter) is in reasonable agreement with the single-electron-loss data up to $q=6$, as shown in Fig. 5. This agreement suggests that the slowly increasing ionization potential has only a small effect on the electron-loss cross section. A similar description of double-electron loss yields

$$\sigma_{2-\text{loss}} = 2\pi \binom{N}{2} \int_0^\infty b\, db\, p_{\text{loss}}(b)^2[1-p_{\text{loss}}(b)]^{N-2}$$

$$= \frac{N!}{(N-2)!2!}\sigma_0. \tag{5}$$

Under the same assumptions employed for the single-electron-loss process, the scaling law becomes $\sigma \sim \frac{1}{2}(N-1)N\sigma_0$. A fit to this scaling law is in good agreement with the double-electron-loss data up to $q=5$, as shown in Fig. 5. The good agreement between this simple electron-loss model, based on the independent-electron approximation, and the data shows that the number of electrons in the outer shell is the most important factor concerning the decrease of electron-loss cross sections with increasing projectile charge.

D. Recoil charge states

The mean recoil-ion charge state as a function of the projectile charge is shown in Fig. 6. It can be seen that the pure target ionization average recoil-ion charge is almost constant. Thus the ionization cross sections for the different final recoil-ion charges increase with q at the same rate. Actually,

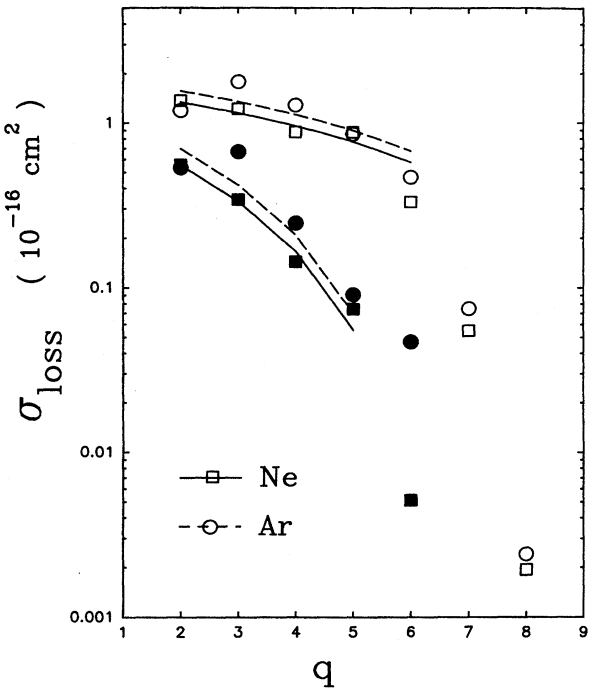

FIG. 5. Single- and double-electron-loss cross sections as a function of projectile charge data. The lines are calculated from scaling laws (see text). Open symbols single-electron loss; full symbols double-electron loss.

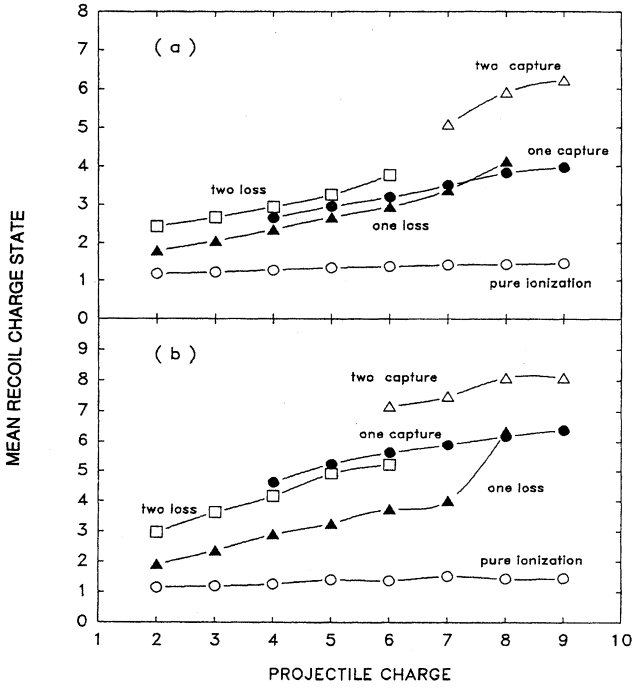

FIG. 6. Mean recoil-ion charge as function of projectile charge (a) Ne target, (b) Ar target.

cross sections for the highly charged recoil ions increase more rapidly than the rest, but these charge states have only a small effect on the mean because their yields are small. This is in agreement with the independent-electron approximation prediction that the ratio of the multiple-ionization cross section to the single-ionization cross section is approximately constant [20]. On the other hand, the mean recoil-ion charge state for electron capture and loss increases rapidly with the projectile charge. The difference in q dependence between pure target ionization and electron-capture or electron-loss processes is associated with the different impact-parameter ranges involved. Pure ionization occurs primarily at large impact parameters, whereas the other two processes are dominant at small impact parameters.

For double-electron capture by highly charged projectiles in Ar targets, the recoil-ion charge distribution shifts up relative to that for single-electron capture by about two charge units because of the capture of one electron and the ejection of another when the inner-shell vacancy is filled by Auger decay (as discussed by Levin *et al.* [23]). Most of the electrons, however, are removed by small-impact-parameter ionization, and hence, aside from the shift of two charge units, the shapes of the double- and single-capture recoil-ion distributions are similar.

ACKNOWLEDGMENTS

This work was supported by the Division of Chemical Sciences, Office of Basic Energy Sciences, Office of Energy Research, U.S. Department of Energy, and by the Robert A. Welch Foundation.

[1] C. L. Cocke, Phys. Rev. A **20**, 749 (1979).
[2] T. J. Gray, C. L. Cocke, and E. Justiniano, Phys. Rev. A **22**, 849 (1980).
[3] H. Dausgaard, H. K. Haugen, P. Hvelplund, and H. Knudsen, Phys. Rev. A **27**, 112 (1983).
[4] A. Muller, B. Schuch, W. Groh, E. Salzborn, H. F. Beyer, P. H. Mokler, and R. E. Olson, Nucl. Instrum. Methods B **24/25**, 11 (1987).
[5] H. Tawara, P. Richard, K. A. Jamison, T. J. Gray, J. Newcomb, and C. Schmiedekamp. Phys. Rev. A **19**, 1960 (1979).
[6] H. Tawara, Phys. Lett. **71A**, 208 (1979).
[7] A. Muller, B. Schuch, W. Groh, E. Salzborn, H. F. Beyer, P. H. Mokler, and R. E. Olson, Phys. Rev. A **33**, 3010 (1986).
[8] H. Knudsen, H. K. Haugen, and P. Hvelplund, Phys. Rev. A **23**, 597 (1981).
[9] N. Bohr and J. Lindhard, K. Dan. Vidensk. Selsk. Mat-Fys. Medd **28**, No. 7 (1954).
[10] A. S. Schlachter, J. W. Stearns, W. G. Graham, K. H. Berkener, R. V. Pyle, and J. A. Tanis, Phys. Rev. A **27**, 3372 (1983).
[11] D. S. F. Crothers and N. R. Todd, J. Phys. B **13**, 2277 (1980).
[12] S. Datz, R. Hippler, L. H. Andersen, P. F. Dittner, H. Knudsen, H. F. Krause, P. D. Miller, P. L. Pepmiller, T. Rosseel, R. Schuch, N. Stolterfoht, Y. Yamazaki, and C. R. Vane, Phys. Rev. A **41**, 3559 (1990).
[13] S. H. Be, T. Tonuma, H. Kumagai, H. Shibata, M. Kase, T. Kambara, I. Kohno, and H. Tawara, J. Phys. B **19**, 1771 (1986).
[14] W. G. Graham, K. H. Berkner, E. M. Bernstein, M. Clark, R. H. McFarland, T. J. Morgan, A.S. Schlachter, J. W. Stearns, M. P. Stockli, and J. A. Tanis, J. Phys. B **18**, 2503 (1985).
[15] J. H. McGuire and L. Weaver, Phys. Rev. A **16**, 41 (1977).
[16] O. Heber, R. L. Watson, G. Sampoll, and B. B. Bandong, Phys. Rev. A **42**, 6466 (1990).
[17] P. Richard, J. Hall, J. L. Shinpaugh, J. M. Sanders, T. N. Tipping, T. J. M. Zouros, D. H. Lee, and H. Schmidt-Böcking, Nucl. Instrum. Methods A **262**, 69 (1987).
[18] O. Heber, G. Sampoll, R. J. Maurer, B. B. Bandong, and R. L. Watson, Nucl. Instrum. Methods B **40/41**, 197 (1989).
[19] O. Heber, G. Sampoll, R. J. Maurer, E. Moler, R. L. Watson, I. Ben-Itzhak, J. L. Shinpaugh, J. M. Sanders, L. Hefner, and P. Richard, Phys. Rev. A **39**, 4898 (1989).
[20] I. Ben-Itzhak, T. J. Gray, J. C. Legg, and J. H. McGuire, Phys. Rev. A **37**, 3685 (1988).
[21] N. Bohr, K. Dan. Vidensk. Selsk. Mat-Fys. Medd **18**, No. 8 (1948).
[22] K. H. Berkner, W. G. Graham, R. V. Pyle, A. S. Schlachter, and J. W. Stearns, Phys. Lett. **62A**, 407 (1977).
[23] J. C. Levin, C.-S. O, H. Cederquist, C. Biedermann, and I. A. Sellin, Phys. Rev. A **38**, 2674 (1988).